Simulation Details

PLCγ1 promotes phase separation of T cell signaling components

L. Zeng, I. Palaia, A. Šarić, X. Su

SI 1 Simulation details

Setup Simulations, as described in the Methods section, were performed with a fixed number of LAT molecules (200); the LAT:Sos1:Grb2 relative concentration was fixed to 1:1:2 (i.e. 200 Sos1 molecules and 400 Grb2 molecules) while PLCγ1 concentration was varied (from 0 to 600 molecules). The size of the simulation box was also varied so as to simulate different LAT surface densities ρ_{LAT}. A rough estimate of the biologically relevant surface density regime stems from the observation that a LAT protein features in reality a 188-aminoacid filament of full-streched length $\sim 65\,\mathrm{nm}$. The gyration radius of such filament, approximately proportional to the square root of the number of monomers, is therefore of the order of a few nanometers. If the radius $\sigma/2$ of a particle in simulations represents the actual gyration radius, an experimental LAT surface density of the order of $10^2\,\mathrm{molecules}/\mu\mathrm{m}^2$ corresponds to a simulated surface density of the order of $10^{-2}\,\mathrm{molecules}/\sigma^2$. This is the density regime that we probe.

More computationally costly checks were run on a 4 times larger systems, including 800 LAT molecules, to ensure that the most important features emerging from simulations, such as the re-entrant effect from Fig. 6B were not an artifact of finite size. Finite size effects were not relevant, except for densities and times large enough to allow the formation of big clusters, of size comparable with the total number of particles in the box.

Particles were initialized at time 0 at random positions on a square lattice, spanning the whole simulation box. The dynamics evolves in steps sufficiently small (0.001 Lennard-Jones time units) so as to ensure stability in the integration of the equations of motion. Periodic boundary conditions are imposed at the four box walls.

For each point in the parameters space, defined by ρ_{LAT} and by the concentration ratio PLCγ1:LAT, we run 10 (or 5, for times larger than 0.5×10^8 timesteps) different realizations of the dynamics for statistical purposes. Error bars in the shown graphs refer to the standard deviation of the plotted quantity across these different realizations.

Interaction potentials The Weeks-Chandler-Anderson potential used for hard-core repulsion between molecules is the following:

$$U_0(r) = \begin{cases} \epsilon_0 \left[\left(\frac{\sigma}{r}\right)^{12} - 2\left(\frac{\sigma}{r}\right)^{6} + 1 \right] & \text{if } r < \sigma \\ 0 & \text{if } r \geq \sigma \end{cases},$$

where r is the distance between the centers of the two spheres, σ is their diameter, and $\epsilon_0 = 10\,k_{\mathrm{B}}T$.

The cosine-squared potential used for interaction between patches is the following:

$$U(r) = \begin{cases} \epsilon \left[\left(\frac{r_0}{r}\right)^{12} - 2\left(\frac{r_0}{r}\right)^{6} \right] & \text{if } r < r_0 \\ -\epsilon \cos^2\left(\frac{\pi}{2}\frac{r-r_0}{r_{\mathrm{c}}-r_0}\right) & r_0 \leq r < r_{\mathrm{c}} \\ 0 & \text{if } r \geq r_{\mathrm{c}} \end{cases},$$

where $r_0 = 0.05\,\sigma$, $r_{\mathrm{c}} = 0.15\,\sigma$ is the range of attraction, and $\epsilon = 30\,k_{\mathrm{B}}T$.

Bonds and clusters A bond between two molecules is defined by two interacting patches being within range of attraction r_{c}. Two molecules are in the same cluster if and only if they are connected by a path of molecules, such that each molecule forms a bond (as just defined) with the next one. Given the short range and the strength of the interaction, which makes bonds irreversible, clusters are robust against reasonably small variations of the cutoff distance used to define a bond. All the software used in the analysis of simulation results, including clustering, was custom-made.

SI 2 Kinetics

To study the kinetics of clusters formation, and later the composition of clusters, we compute two quantities: average cluster size and average coordination. The average cluster size is defined by the number of LAT molecules present on average in a cluster at a given simulation time, for a given point in the parameters space. This corresponds to the total number of LAT molecules divided by the total number of clusters, averaged over different realizations. The average coordination, for LAT, PLCγ1, Sos1, or Grb2 molecules, is defined as the number of bonds formed on average by a molecule of that type (i.e. the number of its occupied binding sites). Fig. SI 1 shows the time evolution of these two quantities.

The average coordination (Fig. SI 1B) exhibits a quick relaxation to its long-time value. This is because most of the bonds are formed during the first 10^7

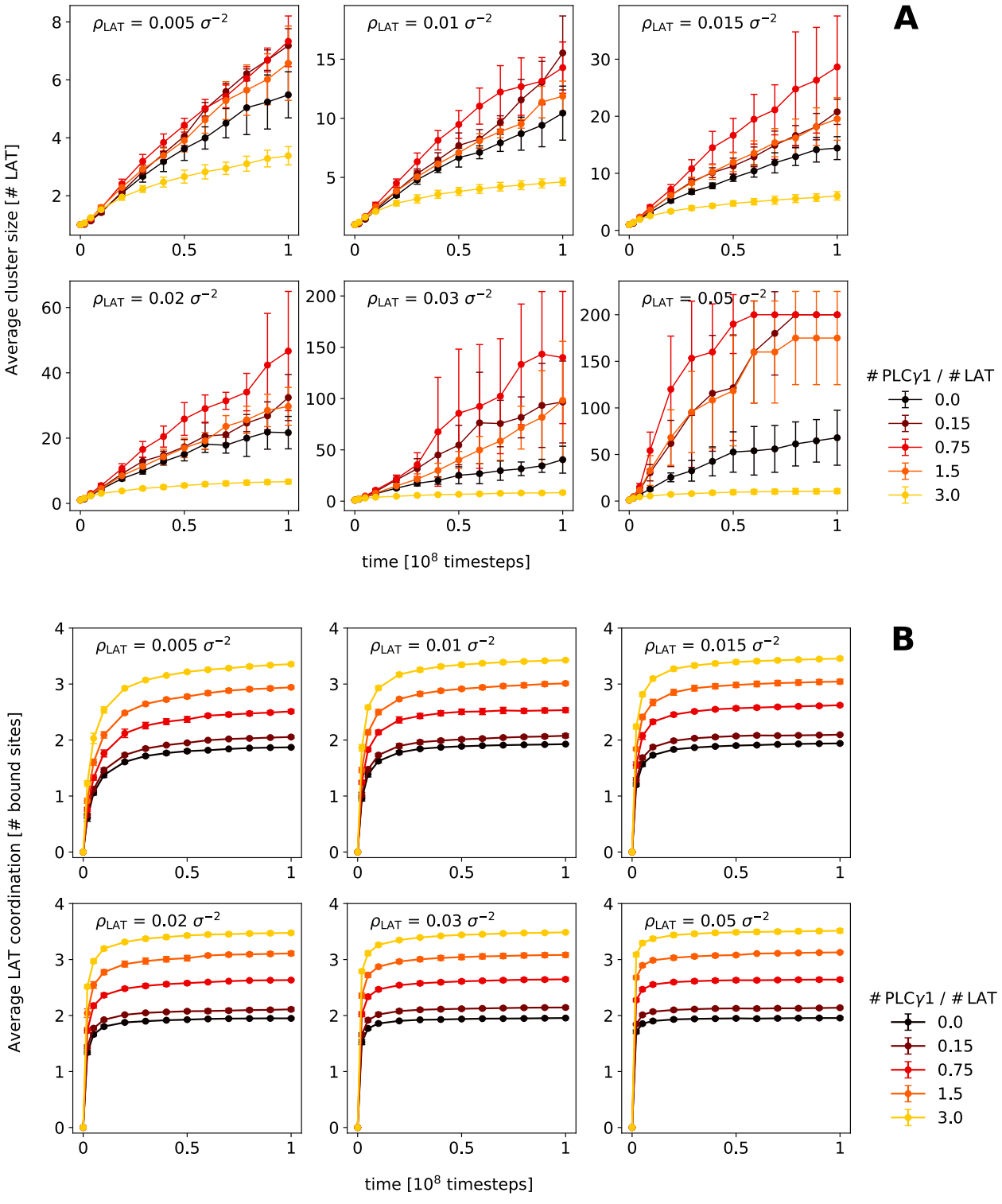

Figure SI 1: Average cluster size (**A**), measured in number of LAT molecules, and average coordination of LAT molecules (**B**), measured in number of bound sites, as a function of simulation time. Different surface densities and different relative PLCγ1:LAT concentrations are shown. In **A**, at large densities, times and cluster sizes, finite size produces large error bars and a likely spurious saturation effect (see Sec. SI 1).

timesteps of the simulations. Later on, bonds become rarer, because many binding sites are already occupied, and because the probability of two particles (or clusters) hitting each other by thermal motion decreases as particles condense locally.

On the other hand, the average cluster size (Fig. SI 1A) is dramatically affected by these late-time binding events, as clusters typically double their size upon binding with one another. At low to medium PLCγ1 concentrations, the curves will ideally grow until all particles are condensed into one big cluster: this is a consequence of irreversible interactions and, ultimately, finite size. In a real system, where bonds can break, the equilibrium cluster size will be set by the balance between bonds dynamics (how often bonds break) and density/entropy (how often clusters bump into each other and new bonds form). On the contrary, at high PLCγ1 concentrations, the linkers saturation phenomenon soon forces the system into a locked state, where further clustering is blocked by the unavailability of binding sites.

An interesting feature of Fig. SI 1A is that plots for different ρ_{LAT} exhibit the same behavior. Surface density seems to act simply as a rescaling parameter and to influence only the rate of cluster formation: the smaller the density, the less frequently clusters will hit each other risking to coalesce. Analogously, in a real system at equilibrium, the smaller the density, the higher will be the entropic cost associated to bond formation.

Even though our simulations are not meant to reproduce quantitative results, but to give a physically sound explanation to observed experimental phenomena, it can be argued that our model represents realistically an early stage of clustering, where the number of particles is low and bonds have not had the time to break yet. Nonetheless, the non-monotonicity of the average cluster size is a persistent feature, present at all simulated times (except obviously very early stages, where most bonds are not formed yet) and at all densities (Figs. SI 2A and 7A). This suggests that the mechanism behind this re-entrant behavior is robust and at least qualitatively independent from time and ρ_{LAT}. Motivated by this observation, in the following (as in the main text) we present in detail data captured at time $t_0 = 0.5 \times 10^8$ steps (when needed, for the sake of conciseness, we also restrict ourselves to a density of $\rho_{\mathrm{LAT}} = 0.02\,\sigma^{-2}$). Our conclusions reasonably hold true, irrespective of this particular choice.

SI 3 Coordination and coalescence

Fig. SI 3 shows average coordinations of all four kinds of molecules, at fixed time t_0. As previously observed, these curves do not depend on density, except for a slight tendency to decrease as density decreases: this is, again, because at equal time, a lower density system has experienced less collisions than a high density one, and this reflects on the dynamics of the coordination curves (see Fig. SI 2B). To help interpret what happens, we focus on $\rho_{\mathrm{LAT}} = 0.02\,\sigma^{-2}$ and break down the four curves from Fig. SI 3, according the the weight of each type of bond. This is done in Fig. 7B, that prompts the following observations.

- The PLCγ1 cSH2 domain compete with the Grb2 SH2 domain for the pY171 site on LAT (top left plot, light orange vs dark blue bar).
- As PLCγ1 concentration increases, LAT's pY132 and pY171 become completely saturated, due to excess of SH2 binding sites from PLCγ1. Remaining pY191 and pY226 are slightly affected: competition with PLCγ1 for pY171 redirect Grb2's SH2 to other LAT sites (medium and light blue bars on gray background), so that overall Grb2 binding to LAT stays constant (gray band in bottom right plot).
- At high PLCγ1 concentrations, Sos1 is completely saturated (bottom left plot), due to the overwhelming abundance of SH3 sites from PLCγ1 (yellow bars). In addition, this SH3 domain on PLCγ1 competes for Sos1 with its homologues on Grb2 (light blue bars on pink background), thus causing a decrease in the overall average coordination of Grb2 (bottom right plot).
- Although its presence favors high coordination of LAT and Sos1, and increases in absolute value the number of bonds, PLCγ1's average coordination decreases with concentration (top right plot). This is due to scarcity of boundable sites on LAT (gray band), and, to a minor extent, of Sos1 (pink band).

All this provides a straightforward interpretation for Fig. 6C, where the coalescence likelihood is observed to decrease drastically, as Sos1 and LAT saturate. The main effect is due to Sos1, which with its 12 binding combinations (Fig. 6A) is involved in the majority of bonds formed in the system.

SI 4 Shape and compactness

In relation to FRAP experiments, we further analyzed the structure of the networks formed within each cluster, as alluded to in Fig. 6D and in the Methods section. We performed first an analysis of the moments of gyration (or inertia) based on standard Euclidean metric, and then a graph-theoretical analysis based on the connections between molecules rather than on their positions. The latter was motivated by the fact that the geometrical features of our model mainly result from the need to impose bond specificity and exclusivity, and are therefore not necessarily physical. The two analyses are however consistent with each other, showing, as expected, a certain degree of correlation between geometry and network structure.

The mechanical analysis was performed by computing inertia tensors of clusters, relative to their center of mass. To this purpose, since the property of interest was of geometrical and not dynamical origin, all molecules were assigned a unit mass. The center of mass was computed by accounting for periodical boundary conditions during the procedure of clustering analysis. As described in the Methods section, the

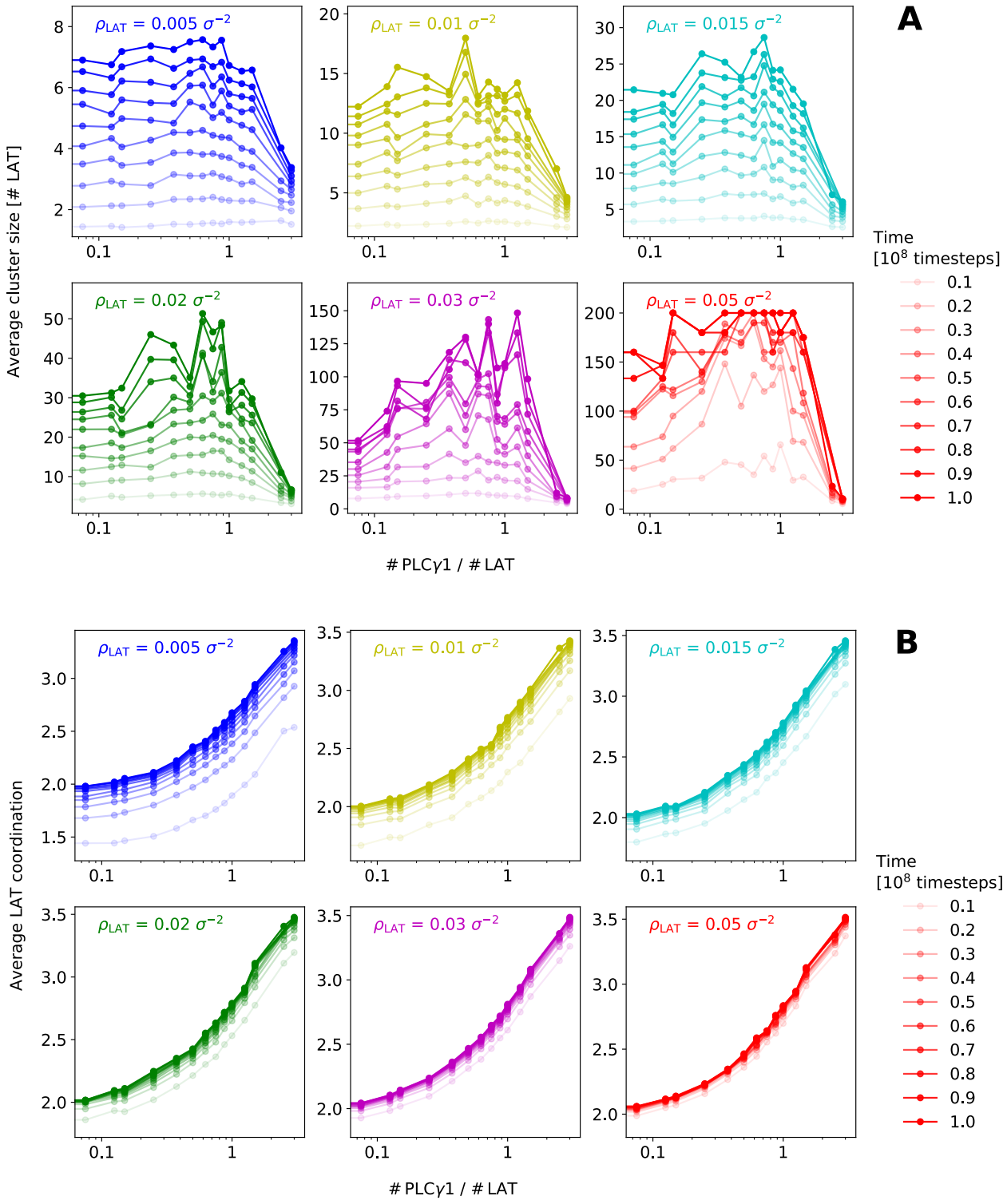

Figure SI 2: Average cluster size (**A**) and average coordination of LAT molecules (**B**), as a function of relative PLCγ1 concentration, at different times and for different surface densities.

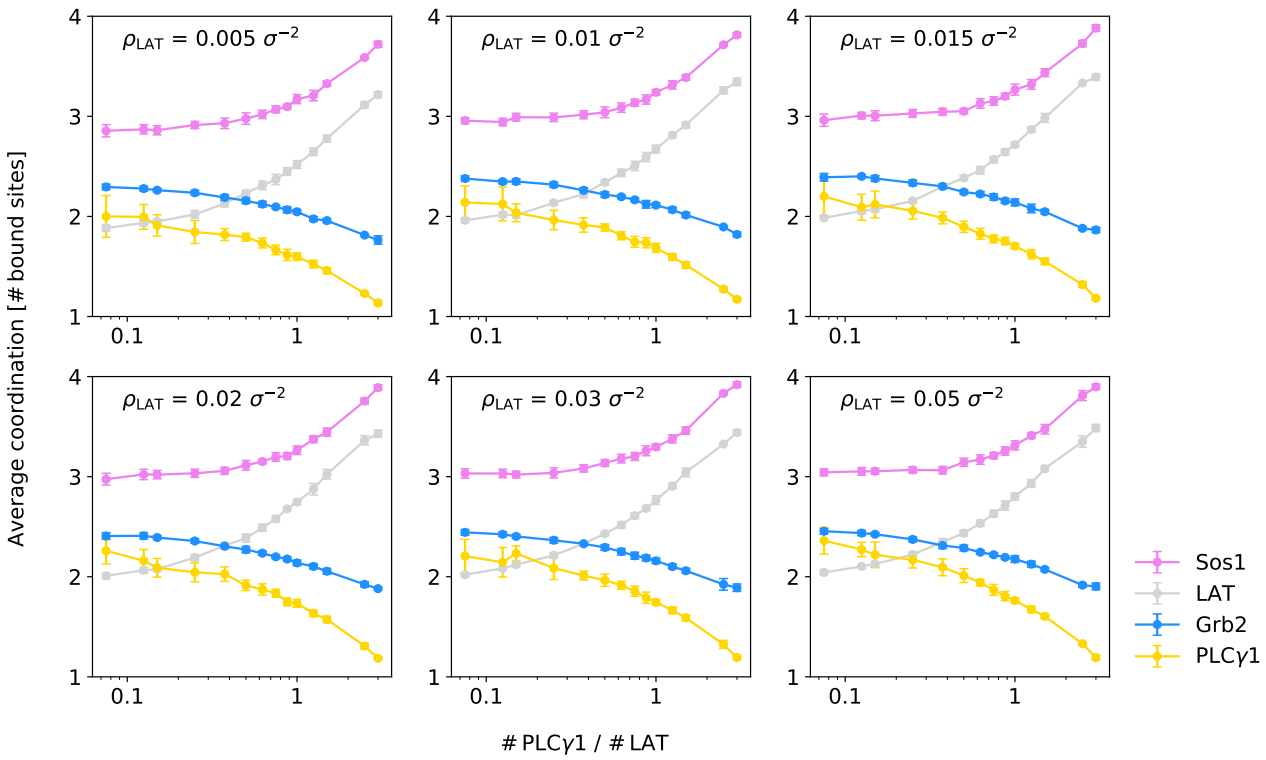

Figure SI 3: Average coordination number for all four kinds of particles, as a function of relative PLCγ1:LAT concentration at time $t_0 = 0.5 \times 10^8$ timesteps. Coordination is defined as the number of bound sites, so it ranges from 0 to 4 for LAT and Sos1, and from 0 to 3 for PLCγ1 and Grb2.

eigenvalues of the inertia tensor I_z, I_1 and I_2 were determined. I_1 and I_2, the squares of the two in-plane gyration radii, were used to quantify two-dimensional shape through a parameter that we called Roundness and defined as follows:

$$\text{Roundness} = \frac{I_1}{I_2}\,, \tag{1}$$

with $I_1 < I_2$. Taking this ratio amounts to approximating each cluster with an ellipse and estimating its eccentricity. The Roundness tends to 0 for clusters in the shape of a straight line and to 1 for in-plane-rotation symmetric clusters, such as circular ones. We then compared the in-plane-rotation principal moment of inertia (I_z) to the same quantity ($I_{z,\min}$) for a homogeneous ellipse of equal roundness, with a density equal to the bulk density of close-packed circles. The latter is the maximum possible density and gives rise to the minimum possible inertia. In practice, for a given cluster,

$$I_{z,\min} = N^2 \frac{\sigma^2}{16\eta} \frac{I_1 + I_2}{\sqrt{I_1 I_2}}\,, \tag{2}$$

where $\eta = \pi/(2\sqrt{3})$ is the packing fraction of a hexagonal close-packed lattice of circles and N is the number of molecules in the cluster. This defines the following Compactness parameter:

$$\text{Compactness} = \frac{I_{z,\min}}{I_z}\,. \tag{3}$$

This Compactness intuitively quantifies the presence of holes in the cluster structure: it is 1 if particles are maximally packed (this is impossible in our case, due to the geometry of bonds, so that the achievable Compactness limit is actually below 1), whereas it tends to 0 for a sparse cluster, with many void regions.

Roundness and Compactness, averaged over clusters mixed up from all different realizations, are shown in Fig. SI 4. Once again, ρ_{LAT} does not seem to play a role. An effect of PLCγ1 concentration on the Roundness is not recognizable: this would require a symmetry breaking phenomenon that does not seem plausible. On the other hand, Compactness increases with PLCγ1 concentration, as observed in the main text.

The graph-theoretical analysis was performed by defining for each cluster an equivalent undirected unweighted graph, where nodes correspond to particles and edges connect two nodes whose corresponding particles are linked by at least one bond. We characterized the sparsity of such graphs by computing the ratio between number of edges $|E|$ and number of nodes $|V| = N$. Indeed, a sparse graph will exhibit a linear proportionality between these two quantities, whereas for a fully connected graph $|E| \sim |V|^2$. Surprisingly, although this ratio cannot exceed 2 in our system because of limited particle valence, it does not show any appreciable increase with PLCγ1 concentration. This is in apparent contradiction with the fact that clusters appear more compact as PLCγ1 is added. The reason is that, due to saturation, most of the added PLCγ1 molecules form only one bond, as confirmed by Figs. 6E and 7B, thus increasing the number of nodes with just one edge (terminal nodes or 'leaves'). This effect is

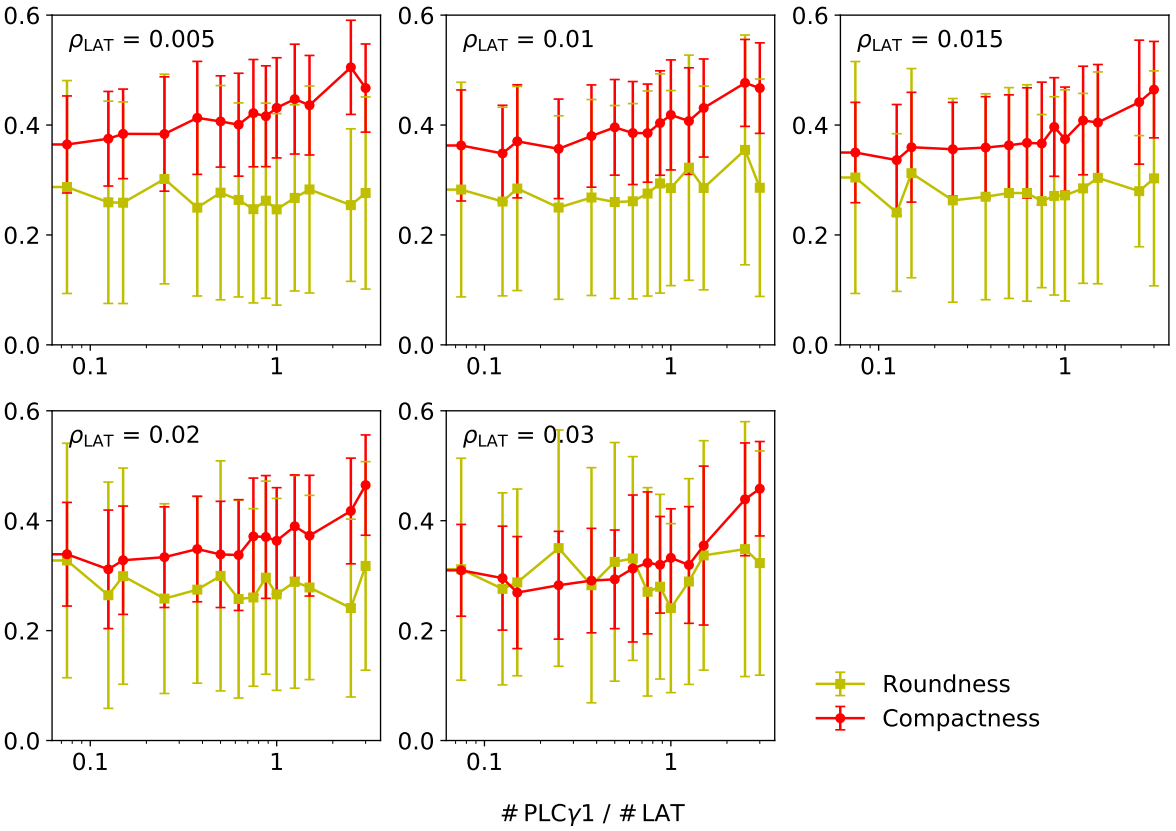

Figure SI 4: Average Roundness and average Compactness as a function of PLCγ1 concentration, for different surface densities. Here error bars represent the standard deviation across all clusters mixed up from different realizations. Only clusters bigger than 30 molecules are considered, to avoid undesired small-size effects.

compensated by an increase in the coordination of LAT and Sos1 (see again Figs. 6E and 7B). The result is a constant sparsity. This observation is coherent with and reinforces our picture of available-bonds-limited cluster growth, symbolized by a decreasing coalescence likelihood.

Finally, we attempted to provide a graph-theoretical equivalent to the Compactness parameter defined earlier on a mechanical basis. We defined a graph-theoretical moment of inertia about the center of mass ($I_{z,\mathrm{GT}}$): this exploits on the one hand the concept of graph-theoretical distance $d(u,v)$, i.e. the number of edges forming the shortest possible continuous path between nodes u and v, and on the other hand the fact that the moment of inertia relative to the center of mass is the smallest one possible (a corollary of the Huygens–Steiner theorem). The graph-theoretical moment of inertia is given by

$$I_{z,\mathrm{GT}} = \min_{u\in V}\left(\sum_{v\in V} d^2(u,v)\right), \tag{4}$$

where V is the set of nodes. This needs to be compared to a similar quantity for a compact cluster; since the latter will scale as $|V|^2$, for simplicity we define the graph-theoretical compactness as

$$\frac{|V|^2}{I_{z,\mathrm{GT}}}, \tag{5}$$

to be compared to Eq. (3). The average of this quantity is plotted in Fig. SI 5 (blue) and increases with PLCγ1 concentration, as expected.

Another measure of the compactness of our graphs originates from the comparison between the diameter D of a graph (the distance between the two most distant nodes) and its theoretical lower bound, approximately given by the Moore limit for vertices of maximum degree 4:

$$D_{\mathrm{Moore}} = \log_3\left(1 + \frac{|V|-1}{2}\right). \tag{6}$$

The average of the quantity

$$\frac{D_{\mathrm{Moore}}}{D} \tag{7}$$

is shown in green in Fig. SI 5 and qualitatively agrees with both the approaches based on graph-theoretical inertia and on mechanical inertia.

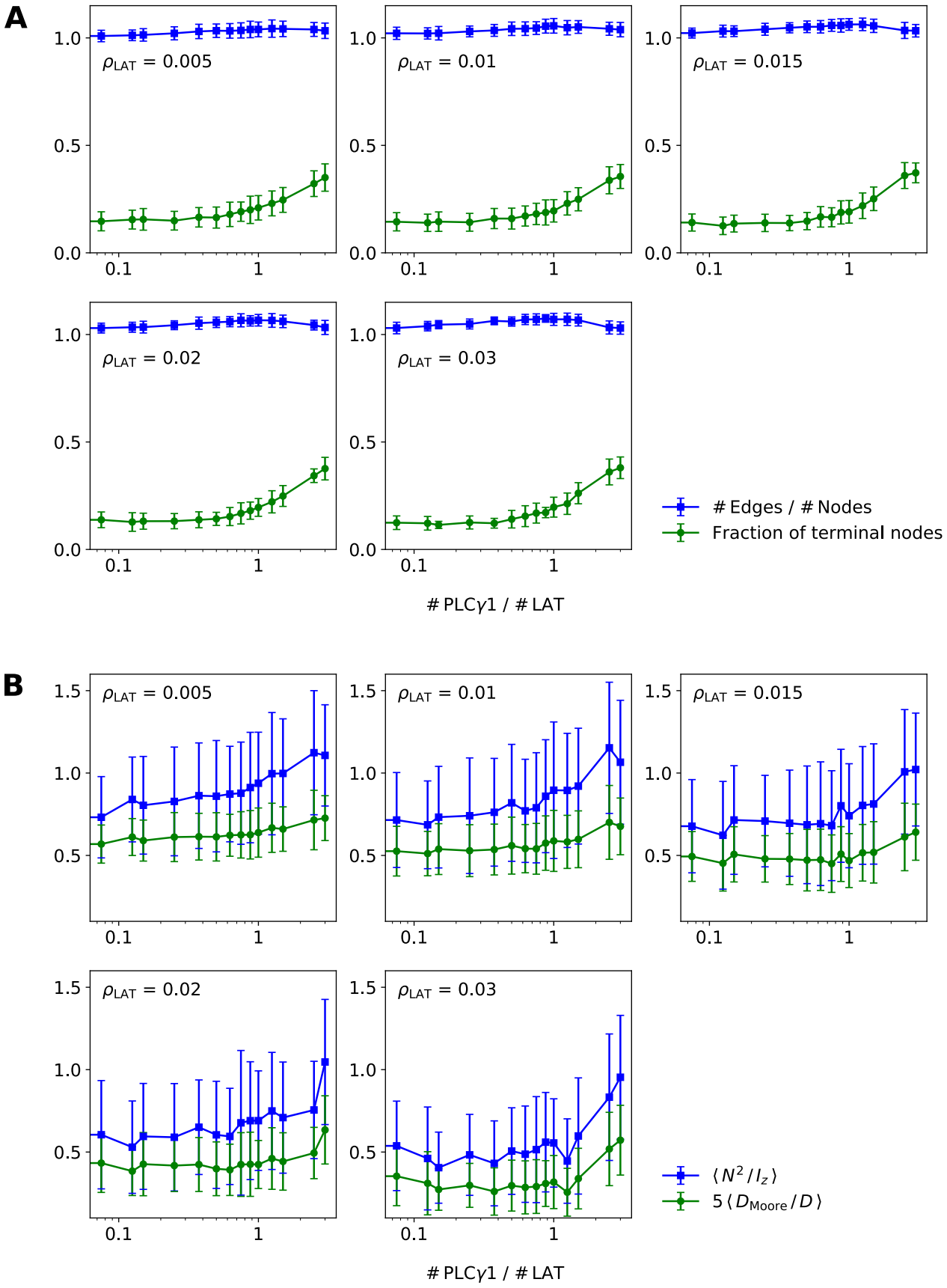

Figure SI 5: **A**. Average sparsity measurement and fraction of terminal nodes as a function of PLCγ1 concentration. **B**. Graph-theoretical characterization of the cluster compactness, through graph-theoretical moment of inertia and diameter, as a function of PLCγ1 concentration, for different surface densities. Error bars and cluster sample as in Fig. SI 4.